Crystal Structures of the Short-Chain Flavin Reductase HpaC from *Sulfolobus tokodaii* Strain 7 in Its Three States: NAD(P)$^+$-Free, NAD$^+$-Bound, and NADP$^+$-Bound[†,‡]

Masahiko Okai, Norio Kudo, Woo Cheol Lee, Masayuki Kamo, Koji Nagata, and Masaru Tanokura*

Department of Applied Biological Chemistry, Graduate School of Agricultural and Life Sciences, University of Tokyo, 1-1-1 Yayoi, Bunkyo-ku, Tokyo 113-8657, Japan

Received November 11, 2005; Revised Manuscript Received March 10, 2006

ABSTRACT: 4-Hydroxyphenylacetate (4-HPA) is oxidized as an energy source by two component enzymes, the large component (HpaB) and the small component (HpaC). HpaB is a 4-HPA monooxygenase that utilizes $FADH_2$ supplied by a flavin reductase HpaC. We determined the crystal structure of HpaC (ST0723) from the aerobic thermoacidophilic crenarchaeon *Sulfolobus tokodaii* strain 7 in its three states [NAD(P)$^+$-free, NAD$^+$-bound, and NADP$^+$-bound]. HpaC exists as a homodimer, and each monomer was found to contain an FMN. HpaC preferred FMN to FAD because there was not enough space to accommodate the AMP moiety of FAD in its flavin-binding site. The most striking difference between the NAD(P)$^+$-free and the NAD$^+$/NADP$^+$-bound structures was observed in the N-terminal helix. The N-terminal helices in the NAD$^+$/NADP$^+$-bound structures rotated ca. 20° relative to the NAD(P)$^+$-free structure. The bound NAD$^+$ has a compact folded conformation with nearly parallel stacking rings of nicotinamide and adenine. The nicotinamide of NAD$^+$ stacked the isoalloxazine ring of FMN so that NADH could directly transfer hydride. The bound NADP$^+$ also had a compact conformation but was bound in a reverse direction, which was not suitable for hydride transfer.

Reduced flavins play important roles as metabolic reaction mediators in a variety of biological processes, including bioluminescence (*1*, *2*), activation of ribonucleotide reductase (*3*), degradation of aromatic compounds (*4*−*7*), synthesis of antibiotics (*8*−*10*), and fossil fuel degradation (*11*). Flavin reductases (FRs) catalyze the reduction of free flavin using NADH or NADPH. FRs can be classified into various subgroups according to their substrate specificities, amino acid sequences, and functional properties. The FRs that use NADH, NADPH, or both are referred to as FRD, FRP, and FRG, respectively (*12*, *13*).

In recent years, a new family of short-chain FRs has been reported (*14*−*17*), with these catalysts acting as small components of two-component monooxygenase systems (Figure 1). The small-component FRs supply reduced flavins to the large component monooxygenases. 4-Hydroxyphenylacetate (4-HPA)[1] 3-monooxygenase is such a two-component enzyme comprising HpaC and HpaB (*17*). HpaC is an NADH:flavin oxidoreductase that supplies $FADH_2$ to HpaB, while HpaB oxidizes 4-HPA to 3,4-dihydroxyphenylacetate (3,4-DHPA) using $FADH_2$, which is the first step of the 4-HPA catabolic pathway (*4*, *18*). 4-HPA is a typical fermented product of aromatic amino acids and some plant materials in animal intestinal tracts, and some bacteria utilize it as a source of carbon and energy (*19*). There is no apparent interaction between the HpaB and HpaC proteins (*20*). To understand the molecular mechanisms of flavin reduction by HpaC and coupled monooxygenation by the partner protein HpaB, we are investigating the structure and function of HpaC and HpaB two-component systems from *Sulfolobus tokodaii* strain 7 (*21*), an aerobic thermoacidophilic crenarchaeon. Here we report the crystal structures of HpaC (ST0723) from *S. tokodaii* strain 7 in its three states, NAD(P)$^+$-free, NAD$^+$-bound, and NADP$^+$-bound, and discuss the environments of FMN and NAD(P)$^+$, the hydride transfer, the conformational changes caused by NAD(P)$^+$ binding, and the substrate specificity.

MATERIALS AND METHODS

Protein Expression and Purification. The gene (st0723) encoding the HpaC protein (ST0723) was amplified by PCR using the genomic DNA of *S. tokodaii* strain 7 as the template. The PCR product was digested with *Nde*I and *Bam*HI and ligated into the T7 expression vector pET-28a-(+) (Novagen). The *Escherichia coli* strain Rosetta(DE3) (Novagen) was used as the host for protein expression. The cells were grown in LB media containing 30 μg/mL kanamycin at 310 K. Protein expression was induced with 1 mM IPTG (isopropyl β-D-thiogalactopyranoside) (Wako). After 12 h, the cells were harvested by centrifugation at

[†] This work was supported in part by the National Project on Protein Structural and Functional Analyses of the Ministry of Education, Culture, Sports, Science, and Technology of Japan and by Grants-in-Aid for Scientific Research from the Ministry of Education, Culture, Sports, Science, and Technology of Japan.

[‡] The coordinates and structure factors (PDB codes 2D36, 2D37, and 2D38) have been deposited in the Protein Data Bank.

* To whom correspondence should be addressed. Tel: 81-3-5841-5165. Fax: 81-3-5841-8023. E-mail: amtanok@mail.ecc.u-tokyo.ac.jp.

[1] Abbreviations: 4-HPA, 4-hydroxyphenylacetate; 3,4-DHPA, 3,4-dihydroxyphenylacetate; IPTG, isopropyl -β-D-thiogalactopyranoside; DTT, dithiothreitol; RMSD, root mean square deviation; NMN, nicotinamide mononucleotide.

10.1021/bi052313i CCC: $33.50
Published on Web 04/04/2006

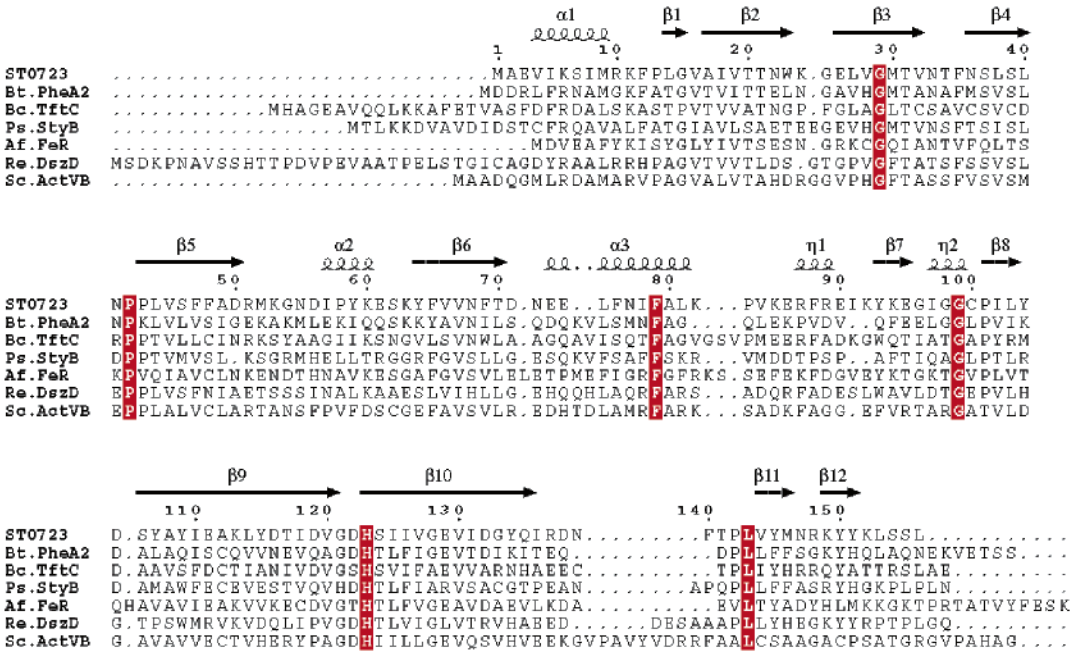

FIGURE 1: Multiple sequence alignment of the homologous proteins of ST0723. Secondary structural elements in ST0723 are indicated above the alignment. Strictly conserved residues among the proteins are shown with a red background. Key: Af.FeR, ferric reductase from *A. fulgidus* (gi 14278202); Ps.StyB, styrene monooxygenase component 2 from *Pseudomonas* sp. (gi 2598027); Sc.ActVB, actinorhodin polyketide putative dimerase from *Streptomyces coelicolor* (gi 14717099); Re.DszD, NAD(P)H:FMN oxidoreductase from *Rhodococcus erythropolis* (gi 11323312); Bc.TftC, chlorophenol-4-monooxygenase component 1 from *Burkholderia cepacia* (gi 3220029); Bt.PheA2, phenol 2-hydroxylase component B from *B. thermoglucosidasius* (gi 7672525).

4500*g* and resuspended in Sol A (50 mM Tris-HCl, pH 7.5, 400 mM NaCl, 5 mM imidazole). The cells were disrupted by sonication and centrifuged at 40000*g* for 30 min. The supernatant was heated at 353 K for 30 min and centrifuged at 40000*g* for 30 min. Then, 0.01% polyethylene imine (Wako) was added, and the resultant supernatant was stirred for 30 min on ice. After centrifugation at 40000*g* for 30 min, the supernatant was loaded onto a Ni-NTA agarose column. The protein was eluted with Sol B (50 mM Tris-HCl, pH 7.5, 400 mM NaCl, 200 mM imidazole). The purified protein solution was dialyzed against 20 mM Tricine, pH 8.5, at room temperature and concentrated to 2 mg/mL using an Apollo 20 mL concentrator (Orbital Biosciences). The protein concentrations were measured by the Bradford method (*22*) using bovine serum albumin as a standard. For the production of Se-Met-labeled protein, the same host strain was grown in minimal M9 medium supplemented with amino acids and selenomethionine. At an OD_{600} of 0.2, expression was induced with 1 mM IPTG (final concentration), and the cells were harvested after 12 h. Dithiothreitol (DTT, a final concentration of 5 mM) was added to all of the buffers except the buffers for the Ni-NTA purification.

Crystallization and Data Collection. Crystallization was performed using the sitting-drop vapor diffusion method at 293 K. Crystals of ST0723 (0.07 × 0.07 × 0.2 mm) were obtained in a day by mixing 1 μL of the protein solution and 1 μL of the reservoir solution containing 7.5% (v/v) 2-propanol and 1.4−1.7 M ammonium sulfate. A drop was equilibrated against 400 μL of the reservoir solution. The $NAD(P)^+$ complex crystals were prepared by soaking the $NAD(P)^+$-free crystal in the reservoir solution supplemented with 50−100 mM NAD(P)H for 15 min at room temperature. The bound flavin stayed reduced for at least 2 h at room temperature. The soaking experiments were performed under aerobic conditions. Se-Met-labeled crystals were obtained under the same conditions as the $NAD(P)^+$-free crystals.

$NAD(P)^+$ complex and Se-Met-labeled crystals were transferred to the reservoir solution containing 25% (v/v) glycerol as the cryoprotectant and flash-cooled at 100 K in liquid nitrogen. Diffraction data were collected in a nitrogen cryostream at beamline BL41XU of SPring-8 (Harima, Japan) and at beamline PF5A of the Photon Factory (Tsukuba, Japan). $NAD(P)^+$-free crystals were mounted in a glass capillary, and X-ray diffraction data were collected at room temperature with an in-house R-AXIS VII (Rigaku, Japan). The diffraction data were indexed and scaled with HKL2000 (*23*). The $NAD(P)^+$-free, NAD^+ complex, $NADP^+$ complex, and Se-Met-labeled crystals belonged to space group $P3_121$ with unit cell dimensions $a = b = 87.6$ Å and $c = 49.6$ Å, $a = b = 86.4$ Å and $c = 49.0$ Å, $a = b = 86.6$ Å and $c = 49.1$ Å, and $a = b = 86.1$ Å and $c = 49.3$ Å, respectively. They contained one HpaC monomer per asymmetric unit according to the Matthews coefficient (*24*). The data statistics are given in Table 1.

Structure Modeling and Refinement. The structure of HpaC was determined by the SAD method using the peak data (wavelength, 0.9790 Å). All of the five expected Se atoms in the asymmetric unit were found using the program SOLVE (*25*). The program RESOLVE (*25*) was used to improve phases. Automated model building was carried out with ARP/wARP (*26*), and approximately 70% of the residues were built. The remainder were built manually with XtalView (*27*) and refined with REFMAC5 (*28*). The $NAD(P)^+$-free structure was then determined by the molecular replacement program MOLREP (*29*) using the Se-Met structure as the initial model. Then, simulated annealing and *B*-factor refinements were performed using CNS (*30*), and further refinements were performed using XtalView and REFMAC5.

Table 1: Data Collection and Refinement Statistics for NAD(P)$^+$-Free, Se-Met-Labeled, NAD$^+$-Bound, and NADP$^+$-Bound HpaC Crystals

	NAD(P)$^+$ free	NAD$^+$ complex	NADP$^+$ complex	SAD selenomethionine
diffraction data				
beamline	in-house R-AXIS VII	Photon Factory BL5A	SPring-8 BL41XU	SPring-8 BL41XU
wavelength (Å)	1.5418	1.0000	0.9840	0.9790
space group	$P3_121$	$P3_121$	$P3_121$	$P3_121$
unit cell parameters (Å)	$a = b = 87.6$, $c = 49.6$	$a = b = 86.4$, $c = 49.0$	$a = b = 86.6$, $c = 49.1$	$a = b = 86.1$, $c = 49.3$
resolution (Å)	50−2.30 (2.38−2.30)	50−1.70 (1.76−1.70)	50−2.05 (2.12−2.05)	50−2.08 (2.15−2.08)
no. of measurements	59629	237246	100597	106364
no. of unique reflections	10047	23559	13622	12984
completeness (%)	99.4 (96.5)	99.9 (100.0)	99.1 (99.4)	98.3 (87.6)
R_{merge}[a]	0.092 (0.308)	0.063 (0.260)	0.052 (0.264)	0.080 (0.192)
$\langle I\rangle/\langle\sigma(I)\rangle$	28.6 (3.46)	66.4 (10.5)	26.4 (4.97)	48.8 (5.10)
refinement statistics				
resolution range (Å)	20−2.30	20−1.70	20−2.05	
R_{cryst}[b] (%)	21.1	17.9	20.4	
R_{free}[c] (%)	24.5	20.0	24.6	
RMS deviations				
bonds (Å)	0.011	0.017	0.008	
angles (deg)	1.284	1.657	1.342	
average B factors (Å^2)				
protein	42.1	22.3	26.1	
FMN	31.7	18.2	28.6	
NAD$^+$		19.6		
NADP$^+$			30.4	
Ramachandran plot				
most favored regions (%)	91.9	94.9	93.4	
additionally favored regions (%)	8.1	5.1	6.6	

[a] $R_{merge} = \sum_{hkl}\sum_i|I_i(hkl) - \langle I(hkl)\rangle|/\sum_{hkl}\sum_i I_i(hkl)$, where $\langle I(hkl)\rangle$ is the average of individual measurements of $I_i(hkl)$. [b] $R_{cryst} = \sum_{hkl}||F_o| - |F_c||/\sum_{hkl}|F_o|$. [c] R_{free} was calculated using 5% of the reflections excluded in the refinement.

Water molecules were added using ARP/wARP. The final model consisted of all of the residues except Lys92, Asn139, Ser155, and Leu156 as well as 18 waters and 1 FMN. Lys92 and Asn139 were refined as Ala because of the lack of their side-chain electron densities. There was no density for the last two residues (Ser155 and Leu156). The NAD$^+$ and NADP$^+$ complex structures were solved by molecular replacement using the NAD(P)$^+$-free structure as the initial model. There were very clear densities for NAD$^+$ and NADP$^+$, respectively. The final NAD$^+$-bound model was composed of 1−155 residues, 84 waters, 1 reduced FMN, and 1 NAD$^+$, while the final NADP$^+$-bound model was composed of 1−156 residues, 56 waters, 1 reduced FMN, and 1 NADP$^+$. Lys92, Asn139, and Leu156 were refined as Ala. The qualities of the models were checked by PROCHECK (*31*). The refinement statistics are shown in Table 1.

Flavin Reductase Assays. Flavin reductase assays were performed in a reaction mixture containing 0.2 μg/mL protein, 50 mM phosphate buffer (pH 7.0), 200 μM NADH or NADPH, and 30 μM FMN, FAD, or riboflavin. Enzyme activity was determined by measuring the decrease in absorbance of NAD(P)H at 340 nm (ϵ_{340} = 6.22 mM^{-1} cm^{-1}). The reaction was initiated by adding NAD(P)H.

RESULTS AND DISCUSSION

Overall Structure. HpaC from *S. tokodaii* strain 7 consists of 156 amino acid residues with a predicted molecular weight of 17965. The crystal structures of HpaC in its three states [NAD(P)$^+$-free, NAD$^+$-bound, and NADP$^+$-bound] were solved at 2.30, 1.70, and 2.05 Å, respectively (Figure 2). The quality of the three structures was assessed by a Ramachandran plot, and no residue in the three structures fell in the generously allowed and disallowed regions. The

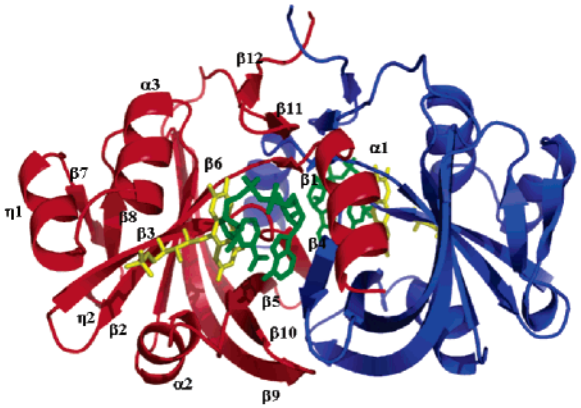

FIGURE 2: Overall structure of HpaC with bound NAD$^+$. Ribbon diagram of the NAD$^+$-bound structure with the two subunits colored red and blue, FMN (reduced form) yellow, and NAD$^+$, green. FMN and NAD$^+$ are represented as sticks.

secondary structure of each monomer was composed of twelve β-strands, three α-helices, and two 3_{10} helices, which formed a seven-stranded β-barrel with a capping α2 helix flanked by the remaining helices and strands. In all three states, HpaC existed as a homodimer (2 × 18 kDa) in the crystal with approximate dimensions of 60 × 40 × 40 Å^3. The molecular weight of the enzyme was determined to be ca. 30000 by gel filtration (data not shown), indicating that it also existed as a homodimer in solution. The two subunits of the homodimer were related by a molecular 2-fold axis. The dimer interface was stabilized by the interactions of the residues located at the α1 helix and β1, β4, β5, β9, β10, β11, and β12 strands. The three structures were very similar to one another with the following pairwise RMSDs (root mean square deviations) for C$^\alpha$ atoms of residues 1−154: 0.93 Å between the NAD(P)$^+$-free and NAD$^+$-bound struc-

tures, 0.89 Å between the NAD(P)$^+$-free and NADP$^+$-bound structures, and 0.15 Å between the NAD$^+$-bound and NADP$^+$-bound structures.

A structural similarity search using DALI (*32*) revealed that HpaC was similar to the following proteins: the styrene monooxygenase small component from *Thermus thermophilus* (19% identical in amino acid sequence; PDB code 1USC; not published) with an RMSD of 2.2 Å for 152 C$^\alpha$, PheA2 from *Bacillus thermoglucosidasius* A7 (27% identical; 1RZ0) (*33*) with an RMSD of 2.2 Å for 144 C$^\alpha$, ferric reductase (FeR) from *Archaeoglobus fulgidus* (25% identical; 1I0R) (*34*) with an RMSD of 2.4 Å for 146 C$^\alpha$, a flavoprotein from *T. thermophilus* (22% identical; 1WGB; not published) with an RMSD of 2.1 Å for 144 C$^\alpha$, and FMN-binding protein from *Methanobacterium thermoautotrophicum* (16% identical; 1EJE) (*35*) with an RMSD of 2.5 Å for 153 C$^\alpha$. The structural comparison of these proteins revealed that the residues on the C-terminal β-sheet, the loop between α3 and η1 helices, and the successive η1 helix contributed to the flavin and NAD(P)H specificities, which will be discussed in detail in the following sections.

Comparison of FMN Binding Sites. The HpaC crystals were yellow, and the electron density map clearly showed that each HpaC subunit tightly bound an FMN. The FMN was located in a pocket near the dimer interface and surrounded by β3, β5, and β11 strands and α2, α3, and η1 helices. The *si* face of the isoalloxazine ring was buried, while the *re* face was completely exposed to the substrates' binding site. The bound FMN was stabilized by 11 hydrogen bonds and hydrophobic interactions (Figure 3). The 2,4-pyrimidinedione moiety of the isoalloxazine ring formed hydrogen bonds with the main-chain atoms of the β5 strand (Phe48 and Asp50) and the side-chain atoms of Thr34 and Asn55. The N5 atom was hydrogen-bonded with the amide nitrogen atom of Asn33. The dimethylbenzene portion of the isoalloxazine ring formed hydrophobic contacts with the enzyme. The ribityl chain of FMN was hydrogen-bonded to the main-chain atoms of Thr31 and Phe79, the N$^\delta$ atom of Asn55, and the N$^{\eta 1}$ and N$^{\eta 2}$ atoms of Arg87. It is likely that the bound FMN is a cofactor because it is tightly bound to the enzyme. Phe79 interacting with the FMN was conserved in the homologous proteins, but many other contact residues were not conserved (Figure 1). There were some water molecules at the NAD(P)H binding pocket in the absence of NAD(P)$^+$, and one water molecule was located above the isoalloxazine ring of the oxidized FMN.

HpaC was found to be most similar to PheA2 (1RZ0) (*33*) of the same short-chain flavin reductase family, but these proteins contained different kinds of flavins, FMN vs FAD. Superimposition of the structures of HpaC and PheA2 revealed that the loop between α3 and η1 helices and the successive η1 helix in HpaC were closer to the bound flavin than those in PheA2. The main chain of Pro83 and Val84 and the side chain of Arg87 caused a steric hindrance to FAD binding so that there was not enough space to accommodate the AMP moiety of FAD in HpaC. Thus, HpaC preferred FMN to FAD.

Comparison of NAD$^+$ and NADP$^+$ Binding Sites. The HpaC crystals were bleached by adding excess amounts of NADH or NADPH, which indicated that HpaC was capable of receiving the hydride from NAD(P)H and of reducing the bound FMN. NAD$^+$ was bound in a cleft formed between

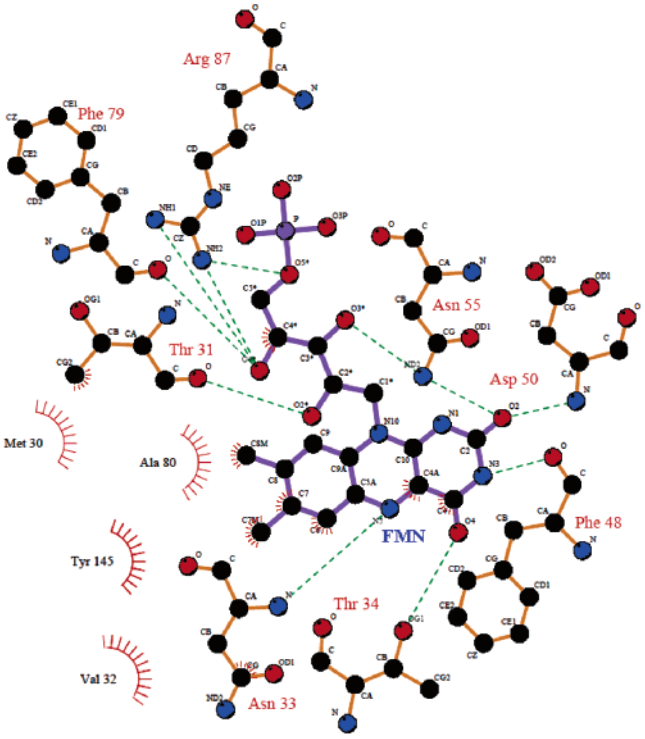

FIGURE 3: Hydrogen bond network between FMN (oxidized form) and HpaC in the NAD(P)$^+$-free structure, which is almost the same as the hydrogen bond network between FMN (reduced form) and HpaC in the NAD(P)$^+$ complex structures. Schematic representation of FMN and the amino acid residues that interact with FMN by potential hydrogen bonds and hydrophobic contacts. Potential hydrogen bonds are represented by dashed lines and hydrophobic interactions by spiked semicircles. The figure was generated using LIGPLOT.

FMN, the N-terminal α1 helix, the β1, β5, β11, and β12 strands, and the β4 strand of the other subunit. The bound NAD$^+$ was hydrogen-bonded with six amino acid residues and several water molecules (Figure 4C). The NMN (nicotinamide mononucleotide) moiety of NAD$^+$ was hydrogen-bonded to N$^\zeta$ of Lys53, N$^\epsilon$ of His123, which was strictly conserved and essential to NAD binding (*36*), O$^\eta$ of Tyr145, and N$^\epsilon$ of Arg148. The 5′-phosphate of AMP was hydrogen-bonded with N$^\eta$ of Arg10 and N$^\eta$ of Arg148. The adenosine moiety was hydrogen-bonded with O$^\gamma$ of Ser37 in the other subunit. The nicotinamide was parallel to the isoalloxazine ring of FMN, and the distance between the C4 atom of the nicotinamide and the N5 atom of the isoalloxazine ring was 3.4 Å, which was close enough for hydride transfer to occur. The bound NAD$^+$ was in a compact folded conformation (Figure 4A) with nearly parallel stacking of the nicotinamide and adenine rings, which was very similar to the conformation of NAD$^+$ bound to PheA2 (*33*). The distance between the adenine C6 and the nicotinamide C2 atoms was only 4.2 Å, indicative of the compactness of the NAD(P)$^+$ conformation (*37*). This conformation is one of the most compact observed to date for NAD(P)$^+$ (*38*). The conformation of NAD$^+$ bound to HpaC was different from the conformation of NADP$^+$ bound to a homologous protein FeR (*34*). The NADP$^+$ in FeR adopted an extended conformation, and the adenine ring was located between the 3_{10}- and the C-terminal α3 helices. However, the C-terminal region in HpaC forms a β-sheet, and the adenine ring of NAD$^+$ was located between the N-terminal residues and the nicotinamide

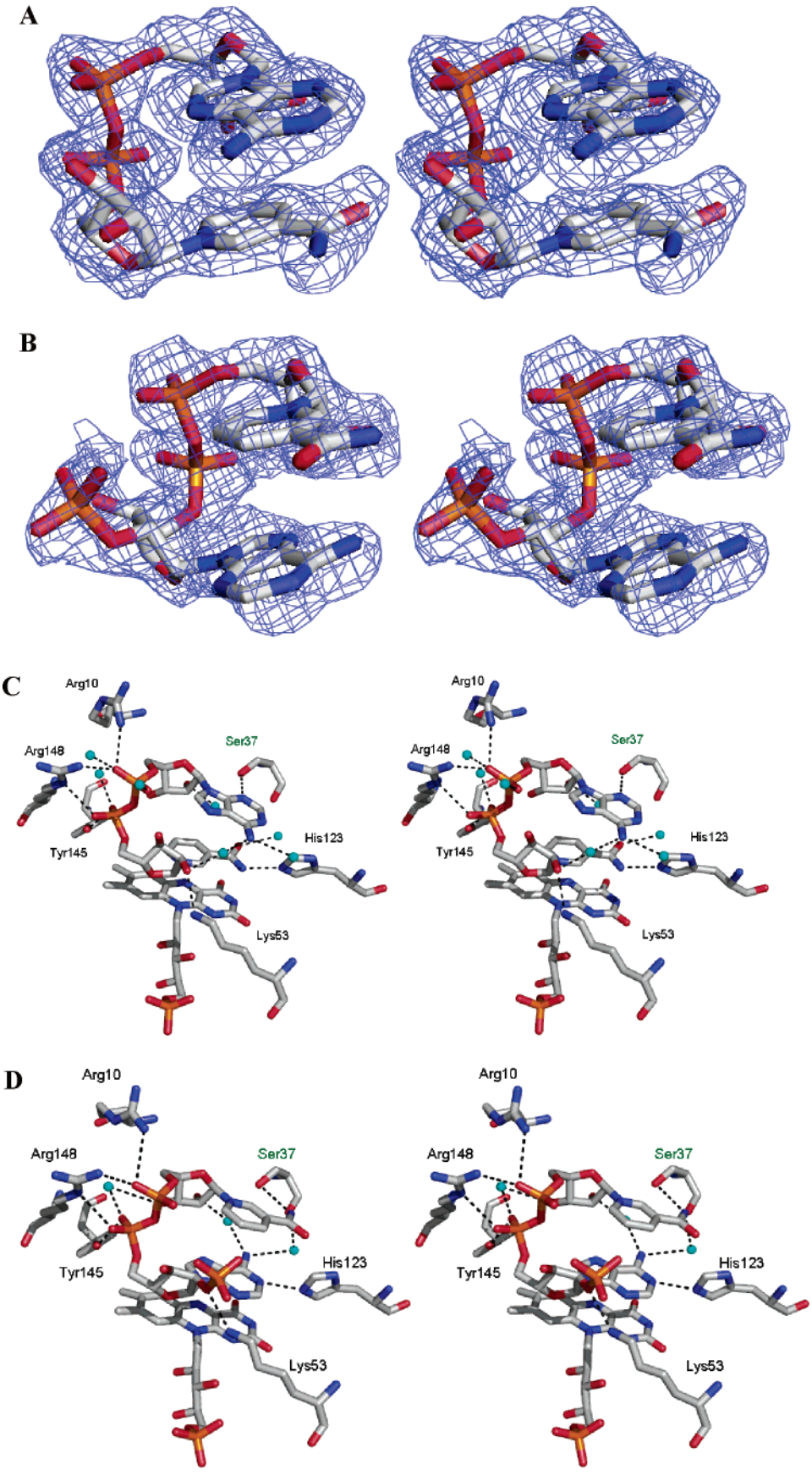

FIGURE 4: $2F_o - F_c$ electron density maps of NAD^+ (A) and $NADP^+$ (B) contoured at 0.8σ with phases computed from the final refine models omitting $NAD(P)^+$. Stereoview of the residues around the NAD^+ (C) and $NADP^+$ (D) binding sites. FMN (reduced form), $NAD(P)^+$, and the amino acid residues interacting with $NAD(P)^+$ are in stick models, and the carbon atoms, oxygen atoms, nitrogen atoms, and phosphate atoms are colored in gray, red, blue, and orange, respectively. Water molecules are colored in cyan. Black dotted lines show potential hydrogen bonds.

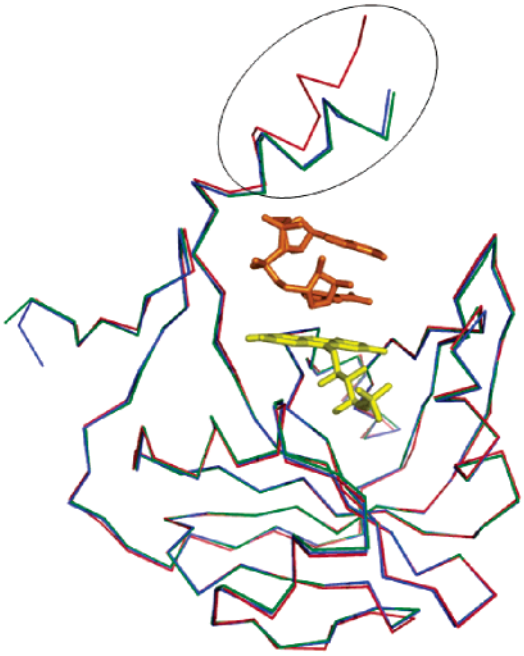

FIGURE 5: Superimposition of the NAD^+- and $NADP^+$-bound enzymes onto the $NAD(P)^+$-free enzyme. Superimposition was performed using the program lsqkab. The $NAD(P)^+$-free, NAD^+-bound, and $NADP^+$-bound enzymes are drawn as α-carbon traces and colored in red, green, and blue, respectively. FMN (reduced in the NAD^+-bound enzyme) and NAD^+ are colored in yellow and orange, respectively. The black circle indicates the N-terminal region.

ring. The bound FMN is in the oxidized form in the $NAD(P)^+$-free structure, while it is in the reduced form in the $NAD(P)^+$ complex structures. The isoalloxazine rings of both the oxidized and reduced FMN were planar, and no conformational changes were observed.

We succeeded in solving the structures of the cryocooled $NAD^+/NADP^+$ complex HpaC, but we failed to refine the structure of the cryocooled $NAD(P)^+$-free HpaC with final $R_{cryst} = 27\%$ and $R_{free} = 33\%$. Thus, we collected the dataset of the $NAD(P)^+$-free HpaC at room temperature using glass capillaries. A C^α superimposition of the three structures is shown in Figure 5. The $NAD(P)^+$-free structure (at room temperature) was very similar to the $NAD^+/NADP^+$ complex structures (under cryocooled conditions), with the most obvious difference being seen at the N-terminal helix. The N-terminal helices of the $NAD^+/NADP^+$ complex structures were tilted ca. 20° relative to that of the $NAD(P)^+$-free structure. Such a conformational change may have occurred due to cryofreezing or by NAD(P)H binding in order to retain the bound NAD(P)H until the hydride transfer occurred from NAD(P)H to FMN.

Although HpaC is an NADH-dependent flavin reductase, the crystal structure of the $NADP^+$-bound HpaC was also solved by soaking the crystal in an excess amount of NADPH. The bound $NADP^+$ adopted a compact folded conformation in which the adenine ring and the nicotinamide ring were stacked (Figure 4B). Unlike NAD^+, however, $NADP^+$ bound upside down in the catalytic pocket. In the NAD^+-bound structure, the distance between the C4 atom of the nicotinamide and the N5 atom of the isoalloxazine ring was 3.4 Å, while in the $NADP^+$-bound structure, the adenine ring lay between the isoalloxazine ring of FMN and the nicotinamide ring of $NADP^+$, and the distance was 7.8 Å, which was too long for direct hydride transfer to occur. In the ferredoxin−$NADP^+$ reductase (FNR), a Tyr residue stacking with FAD must move when the nicotinamide ring of $NADP^+$ interacts with the isoalloxazine ring of FAD (*39*), but such a movement cannot occur in the $NADP^+$-bound structure of HpaC because the adenine moiety is sandwiched between the nicotinamide ring and the isoalloxazine ring.

Table 2: Flavin Reductase Activity

electron acceptor	electron donor	relative activity (%)
FMN	NADH	100
FAD	NADH	65.7
riboflavin	NADH	40.1
FMN	NADPH	5.4

$NADP^+$ interacts with the same residues as NAD^+ (Figure 4D). The adenine moiety was found to be hydrogen-bonded with the side chain of His123. The 2′-phosphate was hydrogen-bonded to N^ζ of Lys53. The pyrophosphate was hydrogen-bonded with the side chains of Tyr145, Arg148, and Arg10. The nicotinamide interacted with the side chain of Ser37 of the other subunit. The NAD^+-bound and $NADP^+$-bound structures were found to be almost identical to each other, with an RMSD of 0.15 Å for C^α atoms of residues 1−154. In the $NAD^+/NADP^+$-bound structures, the residues interacting with $NAD(P)^+$ were located at the same position, meaning that HpaC does not distinguish between the adenine moiety and the nicotinamide moiety of NAD(P)H.

Substrate Specificity. We measured the flavin reductase activity of HpaC to examine its substrate specificity. The reductase activity depended on added NADH or NADPH. As shown in Table 2, HpaC preferred NADH to NADPH as a substrate (NADPH was only 5.4% effective when compared with NADH). On the other hand, FMN was the best substrate among the three flavin compounds. FAD and riboflavin were 65.7% and 40.1% effective, respectively, when compared with FMN.

The $NAD(P)^+$-bound structures of HpaC provide a clue to the NADH dependency of HpaC. In the NAD^+-bound structure, the nicotinamide moiety of NAD^+ stacks the isoalloxazine ring of FMN, whereas in the $NADP^+$-bound structure, $NADP^+$ binds in a reverse direction and the nicotinamide moiety of NAD^+ lies far (7.8 Å) away from the isoalloxazine ring of FMN. If $NADP^+$ could bind in the same fashion as NAD^+, the 2′-phosphate of $NADP^+$ would be buried inside the pocket and surrounded by the side chains of Met9, Leu14, Asn33, Asn36, and Ser37 of the other subunit. Thus, there would be no positive charged residue in this hypothetical 2′-phosphate binding region. It is known that the positively charged residues, such as lysine, arginine, and histidine, play important roles in recognizing the 2′-phosphate of NADPH in NADPH-specific enzymes (*40*, *41*). In the $NADP^+$-bound structure of HpaC, two positively charged residues, Lys6 and Lys53, are positioned at the entrance of the NAD(P)H binding pocket, and these positive charges likely contribute to the reverse mode of binding of $NADP^+$. Lys53 is not conserved in the short-chain flavin reductase family, while Lys6 is conserved as positively charged Arg or Lys (Figure 1).

The specific activity of NADPH-bound HpaC was found to be more than 1 order of magnitude lower than that of NADH-bound HpaC. There are two possibilities regarding the inefficient hydride transfer from NADPH to FMN: (1) a hydride transfers in a long way from the C4 atom of the nicotinamide to the N5 atom of the isoalloxazine ring; (2) a hydride transfers from the small portion of $NADP^+$ that would bind to HpaC, just like NAD^+ to FMN. In the $NADP^+$-bound structure of putative StyB (1USF), the 2′-phosphate of the bound $NADP^+$ was found to be located inside the NAD(P)H binding pocket. Although there is no evidence for multiple conformations of $NADP^+$ bound to HpaC, it is possible that a small portion of $NADP^+$ could bind HpaC in the same manner as NAD^+.

In summary, we have determined the crystal structure of the short-chain flavin reductase HpaC in its three states [$NAD(P)^+$-free, NAD^+-bound, and $NADP^+$-bound]. The structures indicate that (1) HpaC prefers FMN to FAD because of the insufficient space for accommodating the AMP moiety of FAD, (2) NADH and NADPH bind HpaC in the same place but in a reverse direction, and (3) HpaC prefers NADH to NADPH for efficient hydride transfer.

ACKNOWLEDGMENT

Synchrotron radiation experiments were done at SPring-8 (Harima, Japan) (Proposal 2003A0565-NL1-np) and at the Photon Factory (Tsukuba, Japan) (Proposal 03S2-002). We thank Dr. Ohshima (University of Tokushima) for providing us with *S. tokodaii* strain 7 cells.

REFERENCES

1. Zenno, S., Saigo, K., Kanoh, H., and Inouye, S. (1994) Identification of the gene encoding the major NAD(P)H-flavin oxidoreductase of the bioluminescent bacterium *Vibrio fischeri* ATCC 7744, *J. Bacteriol. 176*, 3536−3543.
2. Lei, B., Liu, M., Huang, S., and Tu, S. C. (1994) *Vibrio harveyi* NADPH-flavin oxidoreductase: Cloning, sequencing and overexpression of the gene and purification and characterization of the cloned enzyme, *J. Bacteriol. 176*, 3552−3558.
3. Fontecave, M., Eliasson, R., and Reichard, P. (1987) NAD(P)H: flavin oxidoreductase of *Escherichia coli*. A ferric iron reductase participating in the generation of the free radical of ribonucleotide reductase, *J. Biol. Chem. 262*, 12325−12331.
4. Galán, B., Díaz, E., Prieto, M. A., and García, J. L. (2000) Functional analysis of the small component of the 4-hydroxyphenylacetate 3-monooxygenase of *Escherichia coli* W: A prototype of a new flavin:NAD(P)H reductase subfamily, *J. Bacteriol. 182*, 627−636.
5. Kirchner, U., Westphal, A. H., Müller, R., and van Berkel, W. J. H. (2003) Phenol hydroxylase from *Bacillus thermoglucosidasius* A7, a two-protein component monooxygenase with a dual role for FAD, *J. Biol. Chem. 278*, 47545−47553.
6. Otto, K., Hofstetter, K., Röthlisberger, M., Witholt, B., and Schmid, A. (2004) Biochemical characterization of StyAB from *Pseudomonas* sp. strain VLB120 as a two-component flavin-diffusible monooxygenase, *J. Bacteriol. 186*, 5292−5302.
7. Gisi, M. R., and Xun, L. (2003) Characterization of chlorophenol 4-monooxygenase (TftD) and NADH:flavin adenine dinucleotide oxidoreductase (TftC) of *Burkholderia cepacia* AC1100, *J. Bacteriol. 185*, 2786−2792.
8. Kendrew, S. G., Harding, S. E., Hopwood, D. A., and Marsh, E. N. G. (1995) Identification of a flavin:NADH oxidoreductase involved in the biosynthesis of actinorhodin, *J. Biol. Chem. 270*, 17339−17343.
9. Blanc, V., Lagneaux, D., Didier, P., Gil, P., Lacroix, P., and Crouzet, J. (1995) Cloning and analysis of structural genes from *Streptomyces pristinaespiralis* encoding enzymes involved in the conversion of pristinamycin IIB to pristinamycin IIA (PIIA): PIIA synthase and NADH:riboflavin 5′-phosphate oxidoreductase, *J. Bacteriol. 177*, 5206−5214.
10. Parry, R. J., and Li, W. (1997) An NADPH:FAD oxidoreductase from the valanimycin producer, *Streptomyces viridifaciens*. Cloning, analysis, and overexpression, *J. Biol. Chem. 272*, 23303−23311.
11. Gray, K. A., Pogrebinsky, O. S., Mrachko, G. T., Xi, L., Monticello, D. J., and Squires, C. H. (1996) Molecular mechanisms of biocatalytic desulfurization of fossil fuels, *Nat. Biotechnol. 14*, 1705−1709.
12. Lei, B., Liu, M., Huang, S., and Tu, S. C. (1994) *Vibrio harveyi* NADPH-flavin oxidoreductase: cloning, sequencing and overexpression of the gene and purification and characterization of the cloned enzyme, *J. Bacteriol. 176*, 3552−3558.
13. Tu, S. C. (2001) Reduced flavin: donor and acceptor enzymes and mechanisms of channeling, *Antioxid. Redox Signaling 3*, 881−897.
14. Hüber, A., Danganan, C. E., Xun, L., Chakrabarty, A. M., and Hendrickson, W. (1998) Genes for 2,4,5-trichlorophenoxyacetic acid metabolism in *Burkholderia cepacia* AC1100: Characterization of the tftC and tftD genes and locations of the tft operons on multiple replicons, *Appl. Environ. Microbiol. 64*, 2086−2093.
15. Beltrametti, F., Marconi, A. M., Bestetti, G., Colombo, C., Galli, E., Ruzzi, M., and Zennaro, E. (1997) Sequencing and functional analysis of styrene catabolism genes from *Pseudomonas fluorescens* ST, *Appl. Environ. Microbiol. 63*, 2232−2239.
16. Duffner, F. M., Kirchner, U., Bauer, M. P., and Müller, R. (2000) Phenol/cresol degradation by the thermophilic *Bacillus thermoglucosidasius* A7: Cloning and sequence analysis of five genes involved in the pathway, *Gene 256*, 215−221.
17. Prieto, M. A., and Garcia, J. L. (1994) Molecular characterization of 4-hydroxyphenylacetate 3-hydroxylase of *Escherichia coli*. A two-protein component enzyme, *J. Biol. Chem. 269*, 22823−22829.
18. Xun, L., and Sandvik, E. R. (2000) Characterization of 4-hydroxyphenylacetate 3-hydroxylase (HpaB) of *Escherichia coli* as a reduced flavin adenine dinucleotide-utilizing monooxygenase, *Appl. Environ. Microbiol. 66*, 481−486.
19. Díaz, E., Ferrández, A., Prieto, M. A., and García, J. L. (2001) Biodegradation of aromatic compounds by *Escherichia coli*, *Microbiol. Mol. Biol. Rev. 65*, 523−569.
20. Louie, T. M., Xie, X. S., and Xun, L. (2003) Coordinated production and utilization of $FADH_2$ by NAD(P)H-flavin oxidoreductase and 4-hydroxyphenylacetate 3-monooxygenase, *Biochemistry 42*, 7509−7517.
21. Kawarabayasi, Y., Hino, Y., Horikawa, H., Jin-no, K., Takahashi, M., Sekine, M., Baba, S., Ankai, A., Kosugi, H., Hosoyama, A., Fukui, S., Nagai, Y., Nishijima, K., Otsuka, R., Nakazawa, H., Takamiya, M., Kato, Y., Yoshizawa, T., Tanaka, T., Kudoh, Y., Yamazaki, J., Kushida, N., Oguchi, A., Aoki, K., Masuda, S., Yanagii, M., Nishimura, M., Yamagishi, A., Oshima, T., and Kikuchi, H. (2001) Complete genome sequence of an aerobic thermoacidophilic crenarchaeon, *Sulfolobus tokodaii* strain 7, *DNA Res 8*, 123−140.
22. Bradford, M. M. (1976) A rapid and sensitive method for the quantitation of microgram quantities of protein utilizing the principle of protein-dye binding, *Anal. Biochem. 72*, 248−254.
23. Otwinowski, Z., and Minor, W. (1997) Processing of X-ray diffraction data collected in oscillation mode, *Methods Enzymol. 276*, 307−326.
24. Matthews, B. W. (1968) Solvent content of protein crystals, *J. Mol. Biol. 33*, 491−497.
25. Terwilliger, T. C., and Berendzen, J. (1999) Automated MAD and MIR structure solution, *Acta Crystallogr. D55*, 849−861.
26. Perrakis, A., Morris, R., and Lamzin, V. S. (1999) Automated protein model building combined with iterative structure refinement, *Nat. Struct. Biol. 6*, 458−463.
27. McRee, D. E. (1999) XtalView/Xfit−A versatile program for manipulating atomic coordinates and electron density, *J. Struct. Biol. 125*, 156−165.
28. Murshudov, G. N., Vagin, A. A., and Dodson, E. J. (1997) Refinement of macromolecular structures by the maximum-likelihood method, *Acta Crystallogr. D53*, 240−255.
29. Vagin, A. A., and Teplyakov, A. (1997) MOLREP: An automated program for molecular replacement, *J. Appl. Crystallogr. 30*, 1022−1025.
30. Brünger, A. T., Adams, P. D., Clore, G. M., DeLano, W. L., Gros, P., Grosse-Kunstleve, R. W., Jiang, J. S., Kuszewski, J., Nilges, M., Pannu, N. S., Read, R. J., Rice, L. M., Simonson, T., and

Warren, G. L. (1998) Crystallography & NMR system: A new software suite for macromolecular structure determination, *Acta Crystallogr. D54*, 905−921.
31. Laskowski, R. A., MacArthur, M. W., Moss, D. S., and Thornton, J. M. (1993) PROCHECK: A program to check the stereochemical quality of protein structures, *J. Appl. Crystallogr. 26*, 283−291.
32. Holm, L., and Sander, C. (1993) Protein structure comparison by alignment of distance matrices, *J. Mol. Biol. 233*, 123−138.
33. van den Heuvel, R. H. H., Westphal, A. H., Heck, A. J. R., Walsh, M. A., Rovida, S., van Berkel, W. J. H., and Mattevi, A. (2004) Structural studies on flavin reductase PheA2 reveal binding of NAD in an unusual folded conformation and support novel mechanism of action, *J. Biol. Chem. 279*, 12860−12867.
34. Chiu, H. J., Johnson, E., Schröder, I., and Rees, D. C. (2001) Crystal structures of a novel ferric reductase from the hyperthermophilic archaeon *Archaeoglobus fulgidus* and its complex with $NADP^+$, *Structure (Cambridge) 9*, 311−319.
35. Christendat, D., Yee, A., Dharamsi, A., Kluger, Y., Savchenko, A., Cort, J. R., Booth, V., Mackereth, C. D., Saridakis, V., Ekiel, I., Kozlov, G., Maxwell, K. L., Wu, N., McIntosh, L. P., Gehring, K., Kennedy, M. A., Davidson, A. R., Pai, E. F., Gerstein, M., Edwards, A. M., and Arrowsmith, C. H. (2000) Structural proteomics of an archaeon, *Nat. Struct. Biol. 7*, 903−909.
36. Russell, T. R., and Tu, S. C. (2004) Aminobacter aminovorans NADH:flavin oxidoreductase His140: a highly conserved residue critical for NADH binding and utilization, *Biochemistry 43*, 12887−12893.
37. Bell, C. E., Yeates, T. O., and Eisenberg, D. (1997) Unusual conformation of nicotinamide adenine dinucleotide (NAD) bound to diphtheria toxin: A comparison with NAD bound to the oxidoreductase enzymes, *Protein Sci. 6*, 2084−2096.
38. Tanner, J. J., Tu, S. C., Barbour, L. J., Barnes, C. L., and Krause, K. L. (1999) Unusual folded conformation of nicotinamide adenine dinucleotide bound to flavin reductase P, *Protein Sci. 8*, 1725−1732.
39. Deng, Z., Aliverti, A., Zanetti, G., Arakaki, A. K., Ottado, J., Orellano, E. G., Calcaterra, N. B., Ceccarelli, E. A., Carrillo, N., and Karplus, P. A. (1999) A productive $NADP^+$ binding mode of ferredoxin-$NADP^+$ reductase revealed by protein engineering and crystallographic studies, *Nat. Struct. Biol. 6*, 847−853.
40. Wang, H., Lei, B., and Tu, S. C. (2000) *Vibrio harveyi* NADPH-FMN oxidoreductase arg203 as a critical residue for NADPH recognition and binding, *Biochemistry 39*, 7813−7819.
41. Kobori, T., Sasaki, H., Lee, W. C., Zenno, S., Saigo, K., Murphy, M. E. P., and Tanokura, M. (2001) Structure and site-directed mutagenesis of a flavoprotein from *Escherichia coli* that reduces nitrocompounds: Alteration of pyridine nucleotide binding by a single amino acid substitution, *J. Biol. Chem. 276*, 2816−2823.

BI052313I